BIOMEDICAL MODELLING and simulation
J. Eisenfeld and D.S. Levine (editors)
J.C. Baltzer AG, Scientific Publishing Co. © IMACS, 1989
pp. 133-157

DEVELOPMENT AND APPLICATION OF MATHEMATICAL TECHNIQUES FOR THE NON-INVASIVE LOCALIZATION OF THE SOURCES OF SCALP-RECORDED ELECTRIC POTENTIALS

Robert D. SIDMAN, R. BAKER KEARFOTT, Diana J. MAJOR
Department of Mathematics, University of Southwestern Louisiana, Lafayette, LA 70504, U.S.A.
C. DENSON HILL
Mathematics Department, State University of New York at Stony Brook, Stony Brook, NY 11794, U.S.A.
Martin R. FORD
Psychophysiology Laboratory, The Institute of Living, Hartford, CT 06106, U.S.A.
Dennis B. SMITH, Lu LEE and Ronald KRAMER
Oregon Comprehensive Epilepsy Program, Good Samaritan Hospital, Portland, OR 97210, U.S.A.

Part I: The Mathematical Development of the Dipole Localization Method and the Cortical Imaging Technique

The electrical activity of the brain which is observed on the scalp can be classified under the headings:

A. The oscillating potentials of the brain commonly called the electroencephalogram (EEG), and
B. The potential changes elicited or evoked by external or internal stimuli (evoked potentials or EPs).

The object of the studies described here is to develop and apply mathematical techniques for locating and characterizing the neural generators of such scalp-recorded activity.

1. INTRODUCTION

The localization and description of the neural generators of scalp-recorded potentials, without recourse to invasive diagnostic techniques such as depth or subdural electrodes, is a primary goal of electroencephalography. Additionally, researchers and clinicians try to identify empirical measures for distinguishing "normal" from "abnormal" potential patterns. Since even a specialist can visually identify only dramatic features in an unprocessed sixteen-channel EEG or EP recording, it is necessary to organize the data in such a way that informed inferences can be made.

One way to attain the goals of the localization of neural generators and the discrimination of normal potential patterns is to organize a mathematical-phenomenological model that simulates many of the features of the actual physical setting.

This work was partially supported by a grant from the Oregon Comprehensive Epilepsy Program, Good Samaritan Hospital, Portland, OR.

The dipole localization method (DLM) is one such model. In DLM the head is simulated by a layered conducting medium and the neural generators of scalp-recorded potentials are simulated by a single current dipole. In certain cases the position and direction of the dipole do coincide with the location and orientation of the generators. These cases are distinguished by the fact that the actual generators of these potentials consist of small localized areas of the brain which can be simulated by a single current dipole. Such examples include the application of DLM to the N30-P30 response to median nerve stimulation [1, 2], the scalp potentials generated by a known current source [3], and the sources of certain epileptiform discharges [4].

In other instances, such as the primary cortical responses to pattern-reversal visual stimulation and the N1-P2 complex of auditory vertex potentials, which are generated in rather extensive cortical layers, the DLM solution is more appropriately termed the equivalent dipole generator. For example, the late components of the visual evoked response (VER) are generated, for the most part, in layers of the striate cortex [5, 6]. Various analyses of the N1-P2 complex of responses to auditory stimulation suggest that these potentials are wholly or partially generated in the superior temporal plane, the lateral surfaces of the temporal lobes, and might also include more diffuse frontal cortical sources [7]. Generalizations of DLM allowing for two (or more) dipole sources or dipole layers are possibilities that will be explored in this paper.

From these observations it is apparent that one should not overinterpret a DLM source. In [7] C. C. Wood et al noted that "the number, location and configuration of generators are not uniquely determined by the potential field distribution on the scalp . . . Scalp distributions are important not because they directly specify sources but because they provide a comprehensive characterization of the potentials that must be accounted for by any hypothesized sources and because they provide a basis for testing alternative source hypotheses." This reference notes a common method of analysis that proceeds from the inspection of topographical maps of scalp potential distributions. Presumably the collection of sources and sinks gives some information about the generators of the data. Computationally these maps are usually produced by linear 3- or 4-point interpolation and exhibited in colorful displays. Most of the commercially available imaging machines can also perform simple statistical calculations such as Z-scores in order to compare an evoked response with a collection of normative data.

The DLM method, assuming a single equivalent dipole source, is a parsimonious model that is easy to apply and interpret. It is accurate when one knows in advance that the generator of measured scalp potentials consists of a localized area of the brain. On the other hand, it is unable to distinguish between a deep localized source and a superficial extended source, and it cannot separate discrete but closely spaced sources even when more than one dipole is permitted in the model. Topographical potential maps, as they are currently constructed, are also frequently inadequate to distinguish multiple sources. This is due to the fact that the skull, a highly resistive layer, smears and attenuates the scalp-recorded voltages.

Another component of the mathematical techniques that will be described in this paper offers the possibility of resolving these shortcomings of DLM and topographical analysis. This feature has the effect of approximating the potential distribution on the cortical surface, potentials that have not been smeared and attenuated by the skull. Presumably the cortical topography better preserves a record of current sources and sinks than the scalp topography does.

Mathematically this cortical imaging technique (CIT) is a solution of a harmonic inward continuation problem. The values of a harmonic function are known on the surface of a volume conductor, the head. We show how it is possible to continue this harmonic function into the interior of the head, that is, find the values of the potential inside the head, particularly on the shell modeling the cortical surface.

In the following sections we shall develop the dipole localization method and its generalizations to multiple and extended sources, followed by the development of the cortical imaging technique. We shall illustrate these methods by applying them to clinical or experimental data. Part II of this paper will give applications of DLM and CIT to the localization of epileptic foci and the characterizations of evoked cerebral responses in

normal subjects and certain clinical psychiatric populations.

2. THE DIPOLE LOCALIZATION METHOD (DLM)

2.1. The Inverse Problem of Electroencephalography

Although measured voltages do vary with time, the frequencies of the oscillations are low and the data can be analyzed, as a reasonable approximation, using the principles of potential theory. The analogous localization problem in magneto- encephalography, of course, requires the time dependence of the electric currents for the generation of a magnetic field [8]. Given the assumption of stationarity, the inverse problem can be characterized as follows: suppose potentials are known on the surface S (scalp) of a volume conductor H (head) with conductivity σ; describe the generators (collection of neurons) for these surface potentials.

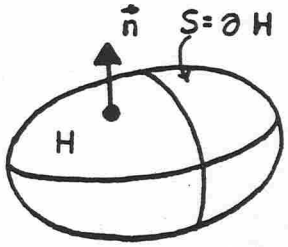

Figure 1

Mathematically the potential V satisfies

$$\nabla(\sigma\nabla V) = F(\vec{x}) \text{ in } H;$$
$$V(\vec{x}) = h(\vec{x}), \quad \frac{dV}{dn} = 0 \text{ on } S, \qquad (2.1.1)$$

where $\vec{x} = (x, y, z)$, values of $h(\vec{x})$ are known, and $F(\vec{x})$ represents the current source density in H.

If the conductivity is constant, then the problem simplifies to:

$$\nabla^2 V = f(\vec{x}) \text{ in } H;$$
$$V(\vec{x}) = h(\vec{x}), \quad \frac{dV}{dn} = 0 \text{ on } S. \qquad (2.1.2)$$

If $v = G(\vec{x}, \vec{x}_0)$ is the Green's function for this problem, then Green's formula

$$\iiint_H (V\nabla^2 v - v\nabla^2 V)\, dH = \iint_S (V\nabla v - v\nabla V)\cdot \vec{n}\, dS \qquad (2.1.3)$$

yields

$$V(\vec{x}_0) = \iiint_H f(\vec{x})G(\vec{x}, \vec{x}_0)\, dH + \iint_S h(\vec{x})\nabla G(\vec{x}, \vec{x}_0)\cdot \vec{n}\, dS . \qquad (2.1.4)$$

The problem is to find $f(\vec{x})$. But h and V are known, in practice, at only a finite number of points, this data is noisy and G is not known for arbitrary regions H. Clearly, it is necessary to make several simplifying assumptions to get a well-posed localization problem.

2.2. The Surface Potentials Produced by a Single Current Dipole in an Insulated Homogeneous Conducting Sphere

The following discussion is taken from [9]. Two point current sources separated by a distance d in an unbounded medium of conductivity produce at a point P the potential $V_\infty = \frac{1}{4\pi\sigma}(I/r_2 - I/r_1)$, where I is the current and r_1 and r_2 are the distances from the two current sources to P. If $d \to 0$ with Id = constant, then $\lim_{d\to 0} V_\infty$ gives the potential of a current dipole located at a point P_0, at the midpoint of the line segment connecting the two original point sources. Such a source can be characterized by six parameters, three giving its location in space and three giving its moments with respect to the three coordinate axes. This type of source can be depicted by an arrow.

In order to find the potential function for a dipole D that lies within a homogeneous insulated sphere, it suffices to construct on the surface of the sphere a double layer whose potential outside the sphere is the negative of the external potential associated with D. The currents and potential function inside the sphere are then the sums of the currents and potential functions for D and the dipole layer [9]. The voltage V(A, D) produced at A, on the spherical surface, by the dipole D can be written in the closed form

$$V(A,D) = \frac{1}{4\pi\sigma} \sum_{i=1}^{3} \frac{m_i}{q_0} \left[\frac{2(a_i - p_i)}{q_0^2} + a_i + \frac{a_i s - p_i}{q_0 + 1 + s} \right], \qquad (2.2.1)$$

where the sphere has radius 1, the coordinates of A are (a_1, a_2, a_3), the dipole D is located at (p_1, p_2, p_3) and has moments with respect to the coordinate axes of m_1, m_2 and m_3, and $q_0 = \left(\sum_{j=1}^{3} (a_j - p_j)^2 \right)^{1/2}$ and $s = \sum_{j=1}^{3} a_j p_j$ [10].

2.3. The Inverse Problem (The Dipole Localization Method)

The equivalent dipole source for measured surface data can be found by minimizing

$$RHO(p_1, p_2, p_3, m_1, m_2, m_3) = \sum_{k=1}^{n} (V(A_k, D) - V(A_k))^2 \Big/ \sum_{k=1}^{n} (V(A_k))^2 \qquad (2.3.1)$$

where n is the number of electrode sites, $V(A_k)$ is the measured potential at A_k, and $V(A_k, D)$ is the theoretical voltage given by (2.2.1).

A more realistic model of the head consists of several concentric layers representing different physiological regions.

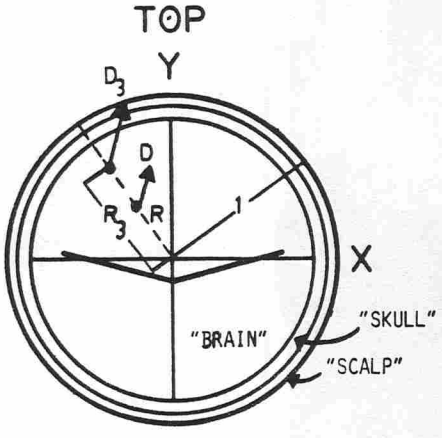

Figure 2

Although V(A, D) no longer has a closed form, the potential still satisfies Laplace's equation at any nonsingular point and can be expanded as

$$V(\theta, \phi, r) = \frac{1}{4\pi\sigma_i} \sum_{n=1}^{\infty} ((A_n^{(i)} r^{-(n+1)} + B_n^{(i)} r^n) P_n(\cos\theta) + (C_n^{(i)} r^{-(n+1)} + D_n^{(i)} r^n) P_n^1(\cos\theta) \cos\phi) \qquad (2.3.2)$$

in the i-th layer, where σ_i is the conductivity of this layer, θ, ϕ, r are spherical coordinates, and P_n and P_n^1 are Legendre polynomials and associated Legendre polynomials, respectively.

At each interface the potentials and radial current densities are continuous and at the outer surface the radial current density dV/dr vanishes. There are just enough boundary conditions to determine the constants $A_n^{(i)}, B_n^{(i)}, C_n^{(i)}$, and $D_n^{(i)}$.

Despite the fact that (2.3.2) is not in closed form, the equivalent dipole source in the 3-layer model of the head, D_3, can be found indirectly from D, the equivalent dipole found above [11]. D_3 can be found by multiplying the coordinates and moments of D by the appropriate correction factors. For example, if R is the distance from D to the center of the sphere and R_3 is the distance from D_3 to the center, then it is approximately true that,

$$R_3 = R \cdot (1.627 - 0.67 R^{2.3}). \quad [12] \qquad (2.3.3)$$

In the following discussion the "theoretical dipole source" or "DLM solution" will always refer to D_3, so that the subscript "3" can be dropped.

2.4. An Application of DLM to the Localization of the Sources of Evoked Potential Components

As an example of the application of DLM to the localization of the source of scalp-recorded potentials, the method is applied to the averaged resting auditory response in a normal subject. Unless we state otherwise, all of the evoked response data in this paper was furnished by the Institute of Living. Scalp recordings were made at twenty-eight electrode sites with a linked ears reference. Stimulus parameters, filter settings, recording conditions and subject/patient description

can be found in Part II of this paper. Our purpose here is to introduce the form in which many results will be exhibited.

As a first step, define

$$P(t) = \left(\sum_{k=1}^{n} V_k^2(t) \right)^{1/2}, \qquad (2.4.1)$$

where $V_k(t) = V(A_k, t)$, the average response recorded at scalp site A_k, t milliseconds poststimulus. Maximum values of P(t), a measure of spatial power, tend to occur at those times (latencies) when there is maximal underlying synchronous neural activity [13]. These times mark some of the most recognizable features or "components" of an evoked response.

In the present case, the graph of P(t) exhibits two power maxima--the first occurring at 124 ms. post-stimulus and the second maximum occurring at 226 ms. post-stimulus. The amplitudes are 28.0μv and 47.4μv, respectively.

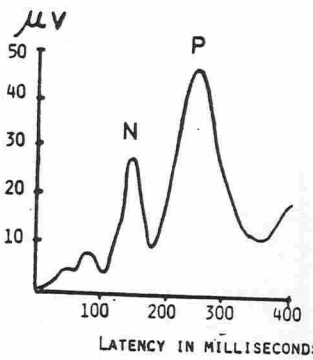

Figure 3

Conventionally the first feature of this response is called the N100 component and the second feature is designated the P200 component, where P and N stand for positive and negative and the numbers are approximate latencies. In the case of auditory responses the polarity refers to the measured voltages at the vertex C_z. (In the case of visual evoked responses, the polarity designation is at the occiput O_z.)

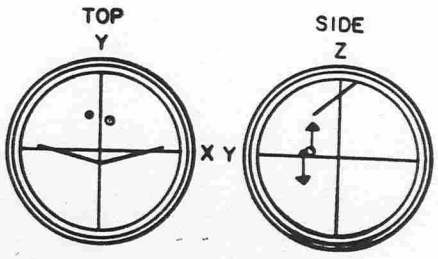

Figure 4

This figure shows the equivalent dipole source for these two components. In this and subsequent illustrations the x-axis goes through the ears, the y-axis passes through the inion and nasion and the z-axis passes through the vertex. The heavy lines in these figures show the approximate location of the central fissure. The equivalent dipole for N100 is the one that points away from the vertex and the equivalent dipole for P200 points toward the vertex. The dipoles that are depicted are actually averages over a 10 ms. time interval. The location and orientation of these sources are stable during these times. The numerical parameters that describe these sources are

Component	x	y	z	m_x	m_y	m_z
N100	-0.12	0.38	.004	-.009	-.03	-.73
P200	0.09	0.32	.02	.0031	.012	.13

Note that these theoretical sources lie near the midline in the interaural plane, not inconsistent with the apparent generation of these potentials in the primary auditory cortex [7].

In practice, the heuristic criterion that we used to decide if a single dipole is a good model for the sources of measured potentials is the condition RHO < 0.1, or, equivalently, -log RHO > 1 (cf. (2.3.1)).

3. MODELS GENERALIZING THE DIPOLE LOCALIZATION METHOD

In several cases it is true that the dipole source corresponds to the actual neural generators of scalp-recorded data, in location and orientation. If the scalp-recorded potentials are generated by a localized synchronous

neural source, RHO is small (< 0.1) during the time epoch when the source is active, and the DLM solution has a stable location and orientation during that time interval, then the DLM solution can be interpreted somewhat literally. In cases when it is clear that multiple or extended sources are involved, the dipole produced by DLM is more properly referred to as an equivalent source. Although the single dipole version of DLM is a parsimonious and easily interpretable model, it is natural to suggest other simulations for the sources of scalp-recorded potentials.

3.1. The Two-Dipole Model for Sources of Scalp-Recorded Data

The N30-P30 response to median nerve stimulation is probably generated in a localized area of the sensory cortex [2, 3]. As a consequence such data was employed to validate DLM. The following figure has been derived from data furnished by the Neuropsychology Laboratory of the West Haven Connecticut Veterans Administration Medical Center.

This figure contains the power curve and scalp topographic maps for left, right and simultaneous bilateral median nerve stimulation, in a patient with a large left occipital-parietal tumor. The scalp topography for bilateral stimulation was produced by algebraically averaging the data from left and right stimulation. These and subsequent surface and contour graphs were generated by using SAS/GRAPH. The stretching in the x-direction is an artifact of the contouring

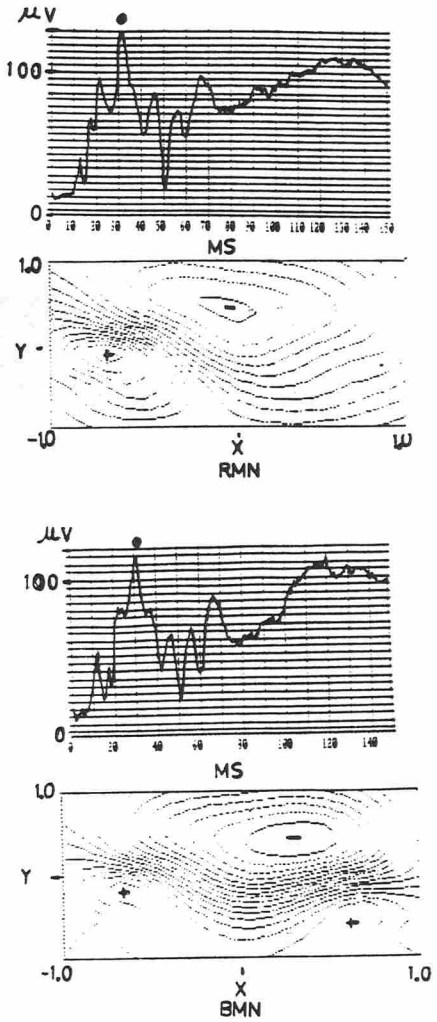

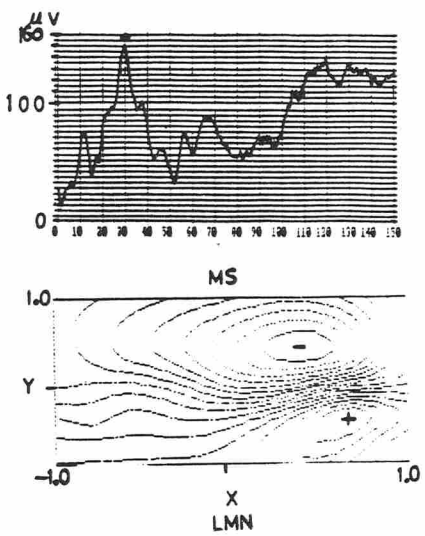

Figure 5

routine. Since the routine fits the point data with cubic splines, the process may occasionally introduce artifactual bumps in the contours, particularly near the edges of the figures. In all of these and subsequent pictures, the plots were scaled to exhibit about 15 equally spaced contours.

From the third topographical map in this figure it is obvious that a single source is a poor model generator. In fact, when DLM is applied to the bilateral median nerve stimulation data, the dipole is stable during a 10 ms epoch containing the 30 ms latency, but RHO is large (> 0.1). This indicates that a single

dipole is inadequate to account for most of the variance in the data (see [14], for example). However, a simple modification of DLM, allowing for two dipole sources, gives the realistic results in Figure 6.

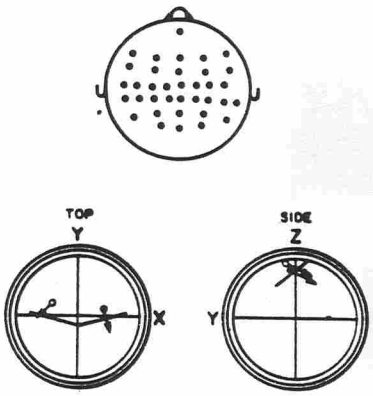

Figure 6

The 36 lead montage, linked ears reference, used at the West Haven VA Medical Center and the dipole pair of sources for the P30-N30 response to bilateral median nerve stimulation are depicted in this figure.

The following example shows one of the limitations of this "generalization" of DLM. The figure shows the scalp topography for the N1 response to visual checkerboard pattern-reversal. This particular case will be discussed at length later in this paper and in Part II.

This response occurs at approximately 96 ms and the scalp topography is virtually unchanging during the 10 ms epoch containing this latency. The single dipole source for this component has stable location and orientation during this time interval and the location and orientation are consistent with the presumed origination of this component in a striate cortical layer underlying the occipital pole. However, RHO is greater than 0.1 indicating that such a source does not account for most of the variance in the data. When the two-dipole version of DLM is applied to this data, the dipole pair is very unstable during the 10 ms epoch. The results for this version of DLM are even physically impossible since one of the dipole pair lies outside the head.

This way of simulating the sources of scalp-recorded data is indicated only when one knows in advance that there are two superficial, widely separated localized neural generators, as indicated by scalp topographic maps. In most other cases, the results do not appear to be useful. The procedure is ill-conditioned or gives nonunique or physically unrealistic results.

3.2. The Dipole Cap Model for Sources of Scalp-Recorded Data

With the exception of cases that have been mentioned above, the actual generators of scalp data probably lie in extended areas of the cortex. In this section neural generators will be modeled by a dipole layer on the boundary of a sphere, rather than by a single current dipole. The particular form of this source is illustrated in Figure 8.

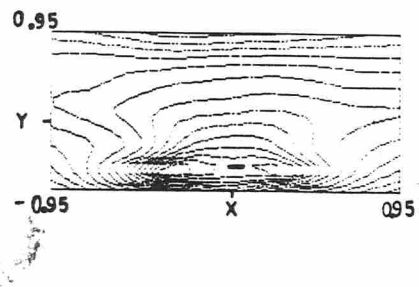

N1 Visual Evoked Potential
Scalp Data
Normal Subject

Figure 7

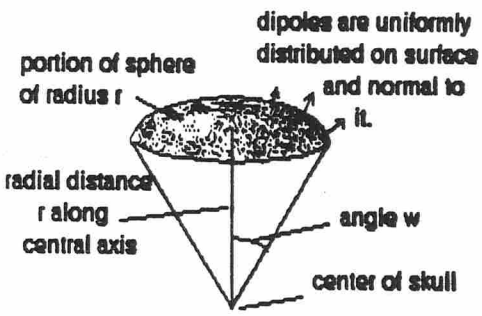

A spherical cap of dipoles.

Figure 8

This type of source is characterized by five parameters: the radius r of the sphere on which the layer lies; a quantity, "intensity," which is a measure of the dipole density of the surface element; spherical angles U and V giving the direction of the central axis of the surface element; and the angle W giving the angular extent of the surface element. The angles U and V are related to Cartesian coordinates in the usual way. If the layer is assumed to lie on the surface of the brain, then r may be fixed and the equivalent layer is determined by four parameters. The inverse problem, assuming such a source is outlined in [15] and [16].

As an application of this method consider the evoked response data in Figures 9A and 9B. The first figure is the power curve for the checkerboard-reversal response from a 28-channel montage, and the source is a normal volunteer at the Institute of Living.

Figure 9B is the response to the same stimulus modality, but for an electrode montage with 6 channels. In this case the source was a normal volunteer at the Naval Submarine Medical Research Laboratory.

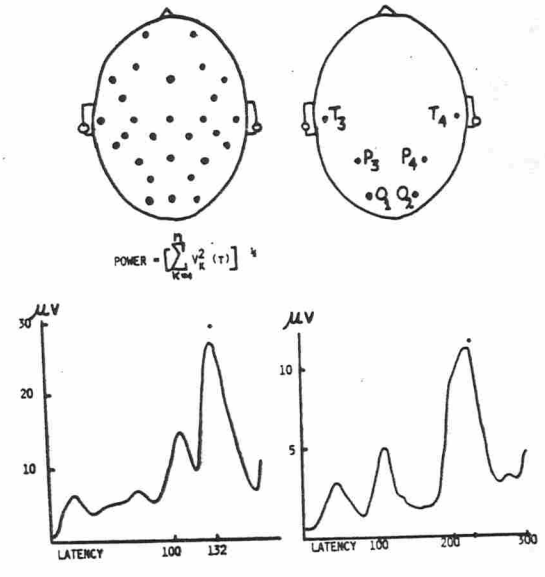

Figure 9A Figure 9B

The next figure shows the equivalent dipole source produced by DLM for each of these cases.

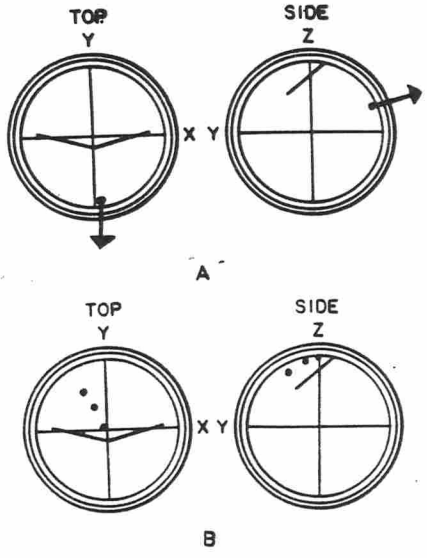

Figure 10

The dipole for the 28-lead data is stable for 10 ms during the epoch containing the indicated component. The equivalent dipole for the six-lead data is very unstable--the localization problem is ill-conditioned in this case when one assumes a single dipole source.

The layer model for this case, however, gives a stable result during a 5 ms epoch. This result is shown in Figure 11.

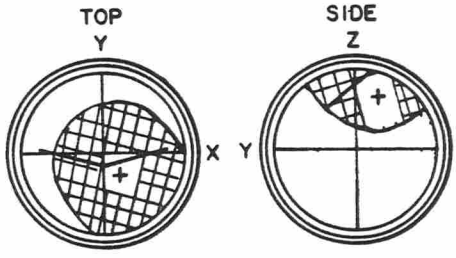

EQUIVALENT SPHERICAL CAP SOURCE FOR THE P2 COMPONENT
6- CHANNEL DATA

R= 0.93 (ASSUMED), THE APPROXIMATE RADIUS OF THE "BRAIN"

LATENCY(MS)	U	V	INTENSITY	W
217.5	-25.6°	15.6°	0.072	95.8°
220	-25.1°	15.1°	0.073	96.2°
222.5	-24.4°	14.2°	0.073	96.5°

Figure 11

We also applied the layer model to two P300 auditory responses (see Part II), one from a normal volunteer and the other a psychiatric inpatient. In one case the equivalent layer was essentially a single dipole and in the other it covered 85% of the area of the shell modeling the cortex.

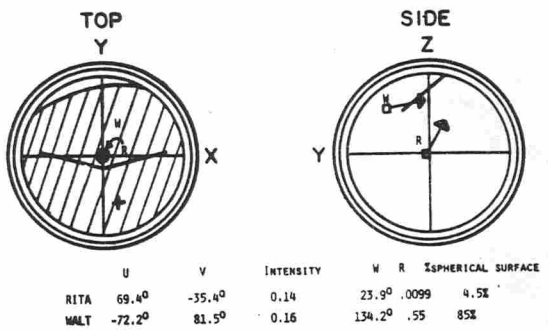

5-Parameter Spherical Cap and DLM Equivalent Sources for Two Auditory P300 Responses. "RITA" Normal Subject; "WALT" Patient

Figure 12

The value of the spherical cap model seems to be that the localization problem is well-conditioned for sparse electrode montages. That is, small changes in scalp-recorded voltages produce only small changes in the equivalent dipole cap. The method employing such layers to simulate neural generators may be useful if only the laterality of brain response is desired.

However, the spherical layer model, having fewer degrees of freedom than the dipole model, is inadequate to characterize multiple sources or extended sources that are not concentric to the surface of the brain. When this model is applied to data generated by such sources, the answer may not be unique or be unrealistic--for example, the cap source for the P300 response of "WALT" covered 85% of the spherical surface.

Since this modeling approach appears to have limited utility, it will not be considered further in this paper.

4. A NEW CORTICAL IMAGING TECHNIQUE FOR STIMULATING CORTICAL SURFACE POTENTIALS

Each of the aforementioned approaches for solving the inverse problem of electroencephalography simulates neural generators in a particular way--with a single dipole, pair of dipoles or a dipole cap. (In [17] two pairs of dipoles are used to simulate the primary source of an auditory evoked response.) But it is apparent that the appropriateness of any such assumption depends upon prior knowledge of the type of source that is present. Scalp topographical maps, as they are presently constructed and analyzed, frequently do not distinguish which type of source is the preferred model. Although DLM, the single dipole version, is an easily implemented method that doesn't suffer some of the problems inherent in the other methods, such as numerical instability, non-unique solutions or physically impossible results, it may not be useful in distinguishing between a deep localized source and an extensive superficial one.

This difficulty derives from the fact that scalp topographical maps frequently fail to exhibit the sources and sinks that would enable one to distinguish single from multiple or extended sources. The skull, a highly resistive layer, smears and attenuates the potential fields generated by sources in the brain. However, if it were possible to place an extensive electrode array directly on the surface of the brain, details of the potential field not discernible on the scalp might appear, perhaps resolving the single source-multiple source-extended source question. We now show how this can be done mathematically to simulate cortical surface data. This cortical imaging technique (CIT) was inspired by an analogue problem in heat transfer described by J. R. Cannon [18].

In Cannon's demonstration a thin rod extending from $x = -\infty$ to $x = +\infty$ was given an initial temperature distribution shown in Figure 13A. The temperature $V(x, t)$ in the rod satisfies the heat equation $V_{xx} = V_t$. When $t = 0.5$, the temperature distribution $V(x, 0.5)$ is shown in Figure 13B. Note that the temperature profile is spreading along the rod and the distinctive features of the initial temperature profile are no longer apparent. When $t = 1.0$, the temperature profile has flattened and spread further and the distinctive double maximum feature of $V(x, 0)$ has apparently disappeared.

Cannon then discretized $V(x, 1)$ and used this discretization $V(x, 1)$ as an initial condition in the heat equation $V_{xx} = V_t$, which he solved numerically backward in time. When t approached 0, $V(x, t)$ recaptured the form of $V(x, t)$, even though noise was allowed in the "initial data," $V(x, 1)$ (Figure 13C). It is important to note that t never equals zero in the backward continuation. The backward problem is not well-posed and has many solutions.

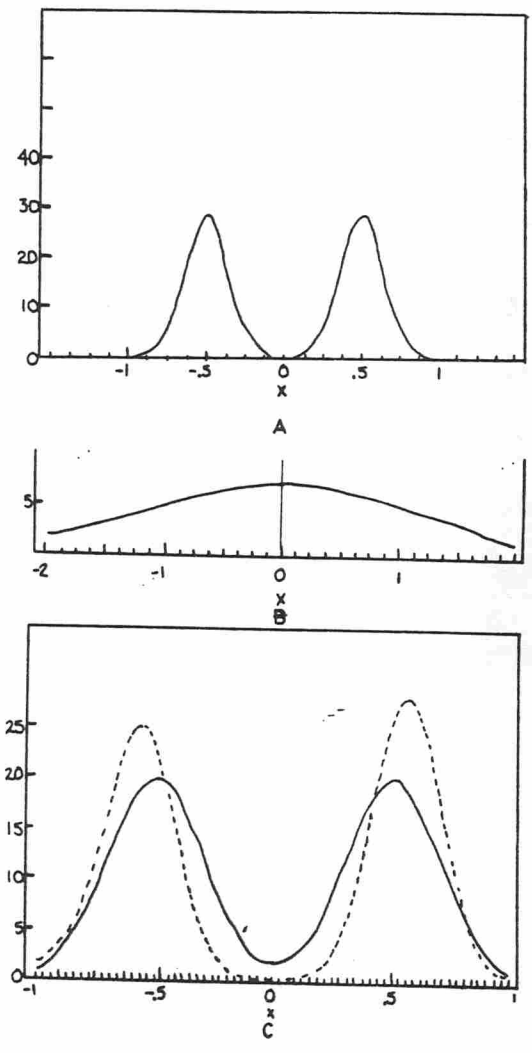

Figure 13

Instead of continuing the temperature function backward in time, our technique is the solution of a harmonic inward continuation problem. The (noisy) values of a harmonic function, scalp potentials, are known on the surface of a folume conductor, the head. We wish to continue this harmonic function to the interior of the head, that is, find the values of the potential inside the head, particularly on the spherical shell simulating the cortical surface.

Like the backward heat problem, this general problem is not well-posed and has an infinite number of solutions. However, we can amend it to a problem that has a unique solution.

Suppose the head is simulated by a homogeneous sphere of radius 1.0, and that N radial dipole sources of unit strength are placed on a test surface of radius r_T. This test surface is a spherical shell concentric to the surface of the "head." A typical dipole of this type D_i is located at $x_i = r_T \cos\theta_i \sin\phi_i$, $y_i = r_T \sin\theta_i \sin\phi_i$, $z_i = r_T \cos\phi_i$ and has moments $\cos\theta_i \sin\phi_i$, $\sin\theta_i \sin\phi_i$, and $\cos\phi_i$, with respect to the coordinate axes.

The potential generated by such a layer can be calculated in the closed form $V(D_i, P_j)$, where P_j lies within or on the unit sphere, using formulas derived by Wilson and Bayley [9]. If $V_1, \ldots, V_M$ are voltages measured at scalp sites $A_1, \ldots, A_M$, it is certainly possible to calculate numbers $u_1, \ldots, u_N$ so that

$$\sum_{i=1}^{N} u_i V(D_i, A_j) = V_j, \quad \text{for } j = 1, \ldots, M. \qquad (4.1)$$

Generally, $M < N$, so that (4.1) is an underdetermined system of equations with an infinite number of solutions. (Most of the applications described in this paper have $M = 28$ and $N = 160$.) However, the solutions for which $u_1^2 + \ldots + u_N^2$ is small will correspond to potential fields with fewer artifactual bumps and wrinkles than solutions for which $u_1^2 + \ldots + u_N^2$ is large. So we seek the unique solution of (4.1) that minimizes the L_2 norm of $(u_1, \ldots, u_N)$. In addition, system (4.1) may be numerically rank-deficient. This suggests that the singular value decomposition method (SVD) can be used to compute the unique solution of (4.1) of minimum norm [19].

An additional advantage of SVD is that it is possible to take account of noise in the data. Given an estimate ϵ_d of the relative errors

in the data, one can replace the system (4.1) by a possibly rank-deficient system such that errors of size ϵ_d will not unduly influence the solution.

Once the values $u_1, \ldots, u_N$ are calculated, the principle of superposition and the aforementioned Wilson-Bayley formulas can be used to compute an approximate image of the potential field on the scalp $r_I = 1$ or any other intermediate spherical shell, $r_T < r_I \leq 1$, including a surface simulating the surface of the brain. Since these formulas can be used to calculate potentials at any point on $r_I = 1$, the topographic scalp maps will be smoother than maps constructed by linear interpolation among only M points. In the applications discussed below and in Part II, scalp and cortical topographical maps are constructed by interpolating 160 potential values on the grid on $r = r_I$ corresponding to the grid on $r = r_T$ on which the test dipoles $D_1, \ldots, D_N$ are placed. The test surface radius r_T has value 0.45 throughout. The radius of the cortical surface is approximately 0.57-0.63, which corresponds to a radius of about 0.90 in the layered model of the head (cf. equation (2.3.3)).

A fuller discussion of this technique can be found in [20]. We are also preparing a careful empirical error analysis of the technique together with applications to artificial and experimental data (R. Baker Kearfott, R.D. Sidman, D. Major, C.D. Hill, in preparation).

The following figures show CIT results for the two examples discussed in Section 3, the response to median nerve stimulation and the response to pattern-reversal checkerboard. A three-dimensional perspective of the potential field and contour maps are shown for each experimental condition on image surfaces whose radii vary from 1 to values near r_T. Note, in particular, the increase in amplitude and detail as r_I decreases. As in the case of the backward heat equation, it is not possible to let $r_I = r_T$ ($t = 0$ in the heat equation case). Spurious artifacts appear if the "recording electrodes" are too close to the current "sources."

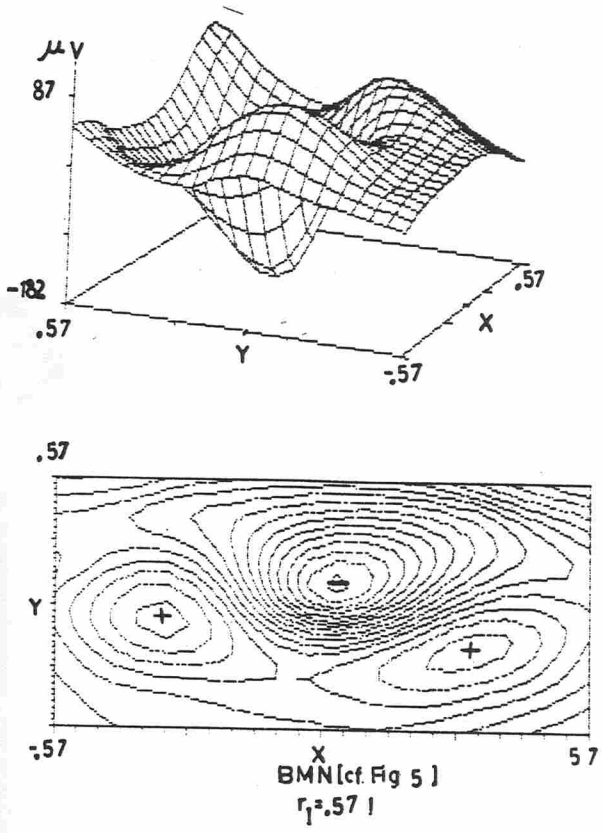

Cortex
Bilateral Median Nerve Stimulation

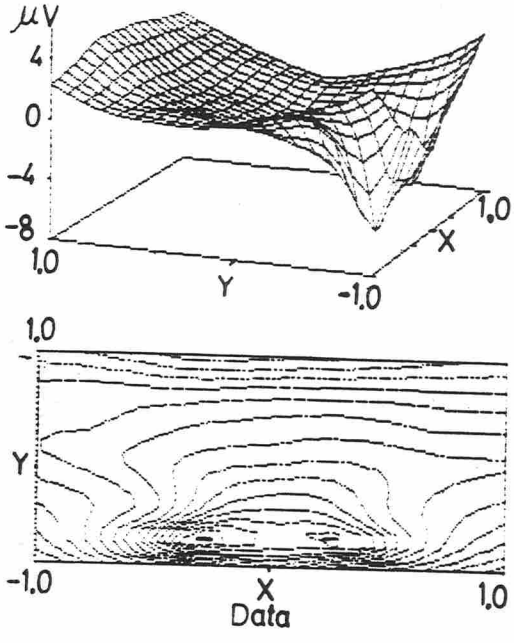

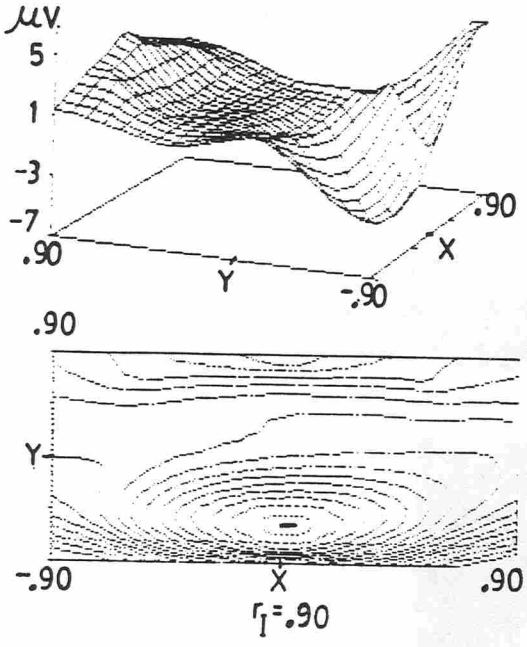

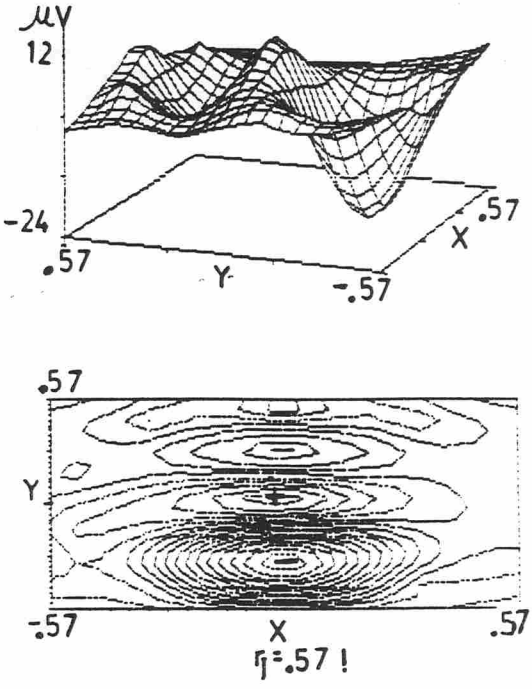

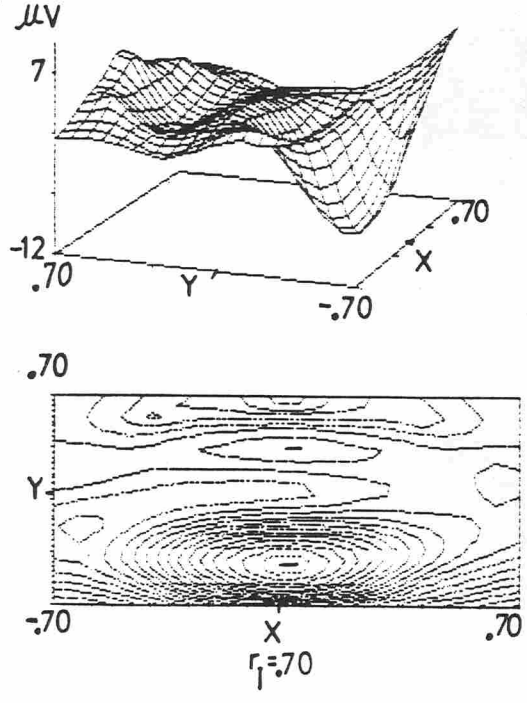

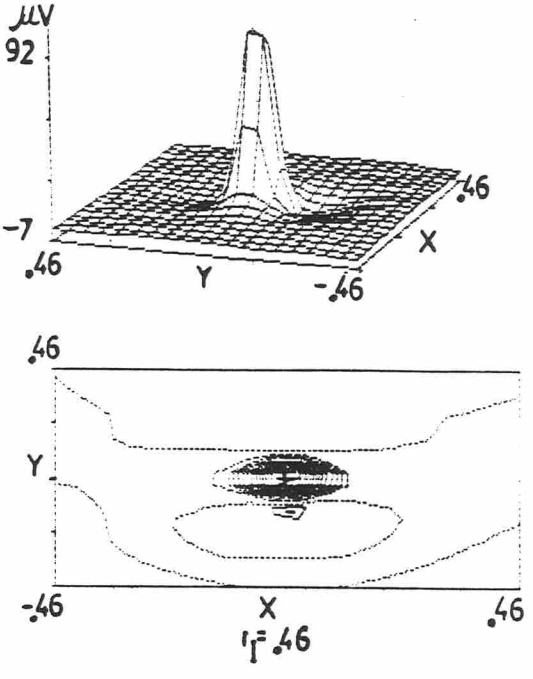

Topography for $0.45 < r_I \leq 1.0$
N1 (VER)

Figure 14

5. CONCLUSIONS

Part I of this paper has described the mathematical development of methods for addressing the so-called inverse problem of electroencephalography. It appears that the dipole localization method (DLM) together with the cortical imaging technique (CIT) are powerful tools for non-invasively identifying and describing the intracerebral sources of scalp-recorded electrical potentials. Part II will demonstrate the value of these mthods in localizing epileptic foci and distinguishing normal and abnormal evoked responses.

Part II: Analysis of Normal and Abnormal Auditory and Visual Evoked Responses Using DLM and CIT and the Localization of Epileptic Foci

In the first part of this paper DLM and CIT are applied to auditory resting and P300 responses and pattern-reversal visual responses from normal volunteers and psychiatric patients. For these modalities it appears that DLM can be used to characterize normal evoked potentials and identify abnormal responses in cases of dysfunction. CIT can be used to indicate why a response is abnormal.

When patients with epilepsy are being considered for surgical therapy, confident localization of the seizure focus is essential. Since there are risks associated with invasive recording techniques such as sphenoidal or depth electrodes, it is desirable to develop methods that require only the acquisition of scalp-recorded data. In the second part of this paper DLM is applied to single interictal spikes and "averaged" interictal spikes in patients being evaluated for epilepsy surgery, and the localization results are compared with known intracranial origins and magnetic resonance imaging results. A single dipole fit the data well (RHO < 0.1) and the localization correlates well with the known epileptogenic focus.

6. APPLICATIONS OF DLM AND CIT TO RESTING AND P300 AUDITORY RESPONSES AND PATTERN-REVERSAL VISUAL RESPONSES IN NORMAL VOLUNTEERS AND CLINICAL POPULATIONS

Various aspects of brain morphology and physiology have been investigated in patients with psychiatric disorders. Earlier quantification procedures have relied on postmortem measurements of brain size, ventricle dilation, left/right differences, gray matter/white matter ratios, etc. More recently, sophisticated in vivo morphological measurements have been possible with contrast CT-scans and magnetic resonance imaging (MRI) techniques. Measurements of more functional properties have been accomplished with conventional and computerized electroencephalographic analyses, regional cerebral blood flow measurement (rCBF) and, most recently, with positron emission tomography (PET). Neuropsychological assessment, a behavioral-based method which allows inferential localization of brain function, has also been used with psychiatric populations.

Recent studies using computerized analyses of brain electrical activity and color display techniques have identified reasonably consistent abnormalities in psychiatric patients, particularly in schizophrenics. In addition to analyzing conventional EEG and resting auditory evoked responses (AER), several studies have focused upon the evolution and topography of the AER P300 waveform. Resting AERs indicate primary and secondary processing of auditory stimuli. In P300 recording paradigms, subjects are instructed to count randomly presented "oddball" stimuli (e.g., a higher pitched tone), and only the responses to the "oddball" stimuli are averaged. The resulting AER shows the usual N1/P2 (N100/P200) complex and an additional prominent positive vertex peak beginning around 300 ms [21]. The P300 is not affected by variations in the stimuli; rather it is contingent upon the subject's concentration and attention, and probably reflects the neurophysiological process associated with the updating of working memory.

In schizophrenic subjects, P300 has been shown to be attenuated in the left temporal area [22, 23]. Research at the Institute of

Living has confirmed the P300 attenuation. However, the attenuation appears more frontally as well and is more consistent with results from other imaging and neuropsychological evaluations. Moreover, the attenuation appears not only in patients having diagnoses of schizophrenia, but also in related disorders in which there are symptoms of thought disorder (e.g., schizophreniform, schizoaffective, major depression with psychotic features). While the attenuation appears in scalp recordings, it has been hypothesized that the site of the abnormality is in the limbic system, and the cortical attenuation reflects underactivation in the ascending aminergic system [22]. Depth recordings from limbic structures (hippocampus) have verified the presence of the P300 component, and have demonstrated unilateral attenuation in depth and scalp P300s in patients with complex partial seizures which are localized to the left or right temporal lobes [24].

The purpose of the first part of this section is to apply DLM and CIT to the analysis of the resting AER and P300 waveforms in normal volunteers and selected patients with thought disorder symptoms and left frontotemporal P300 attenuation. Generally the vertex elextrode C_z is the marker that defines the auditory components N1/P2 and P300. This and the discussions in Part I and reference [7] suggest that the dipole sources for N1 and P2, in normal subjects, should lie in the supratemporal plane (the x-y plane in our geometry), near the midline (the y axis), and be perpendicular to the x-y plane. The equivalent dipole for N1 should be oriented away from the vertex and the equivalent dipole for P2 should be oriented away from the vertex. The equivalent dipole for P300 should be centrically located and point toward the vertex.

The subsequent part of this section gives applications of DLM and CIT to the analysis of the response to pattern-reversal visual stimulation in normal volunteers and alcoholics. In normal subjects one would anticipate that the theoretical dipole source for the principal far-field components should be located near the occipital pole and be oriented toward or away from the nasion in a view of the head from above [6, 25]. Expectations for the DLM sources in the cases of an alcoholic subject are problematic since the category "alcoholic" is a difficult one to define precisely. In the cases presented here there is no good dipole fit at any latency or the dipole source has a direction or location inconsistent with the presumed origins of these components in striate cortex.

6.1. Stimulus and Recording Parameters

All electrical recordings were made with a 28-channel NeuroScience Brain Imager, Series III, with full mapping and statistical capabilities. Stretchable caps (Electro-caps, Inc.) were used for electrode placement. The 10-20 system, with ten additional placements for improved resolution, provided complete coverage of the head. A linked-ears reference was used throughout.

The following lists give recording parameters and filter settings for the three stimulus modalities.

General:

- Analysis time: 600 ms
- Recording sites: 28 scalp recording sites from the International 10-20 System or derivable from these linked ears reference
- Sampling rate: 1 ms and averaged every 2 ms
- Potentials from eight time points prior to the stimulus (tone or pattern-reversal) are averaged and subtracted from the record to produce a 0-baseline
- Dynamic Range: 256μv
- Artifact Rejection: 90% so any voltage response > 115μv or < -115μv is rejected

---

Resting Auditory Evoked Response:

- Low Filter: 0.3 Hz
- High Filter: 40 Hz
- 60 Hz notch filter on

Binaural Stimulus:

- Interstimulus Inverval (ISI), 1 sec.
- Frequency 1 kHz
- Rise-Fall 10 ms
- Plateau is 50 ms total duration with sound pressure level at 90 dB
- 64 trials are averaged

Auditory P300 Response:

Same filter settings

Binaural Stimulus:

- ISI 2 sec.
- Oddball stimulus probability 20%

Frequency 2 kHz
32 trials are averaged

Visual Evoked Response:

Low Filter: 1.05 Hz
High Filter: 40 Hz
60 Hz notch filter on

Stimulus:
ISI 1 sec.
Full Field Checkerboard Reversal-
14" diagonal screen 18" from subject in darkened room, 32 x 32 checks with approximately 1^{o} visual angle

64 trials are averaged

6.2 Subjects

There were 22 normal volunteers who participated in the resting auditory and P300 study, 11 were male and the mean age was 33.3 years. In the visual study there were 21 normal subjects, 10 male, with a mean age of 33.7 years. Several subjects participated in both studies. All volunteers had normal visual and auditory acuity and no record of neurological or neuropsychological impairment.

Evoked potential data from nine psychiatric inpatients (six males; mean age 38.9 years) were selected for the AER and P300 studies. DSM-III diagnoses of the patient group were: schizophrenia, paranoid (n = 1), chronic (n = 2); schizophreniform (n = 3); probable schizophrenia (n = 1), major depression with psychotic features (n = 1) and atypical depression with questionable schizophreniform diagnosis (n = 1). Inpatients' recordings were originally made for clinical analyses and interpretation.

Visual evoked potential data were obtained from nine alcoholic patients (five males; mean age 31.1 years). Each patient was age and sex-matched to a normal volunteer.

Detailed analyses of these clinical applications will appear in forthcoming publications. In the following sections we present the DLM solutions, scalp and cortical topographies for the normative data and for selected abnormal cases. Throughout, subjects are designated by acronyms and not their names.

6.3. DLM and CIT Results for Resting AER and Auditory P300 Responses

Figure 15A is the power curve for the grand average data derived from the 22 normal subjects. The main components of this response appear to be N100 at 122 ms and P200 at 214 ms. Figures 15B and 15C are, respectively, the dipole sources for the grand average data (for N100 and P200) and the average dipole sources for these components for the 22 subjects.

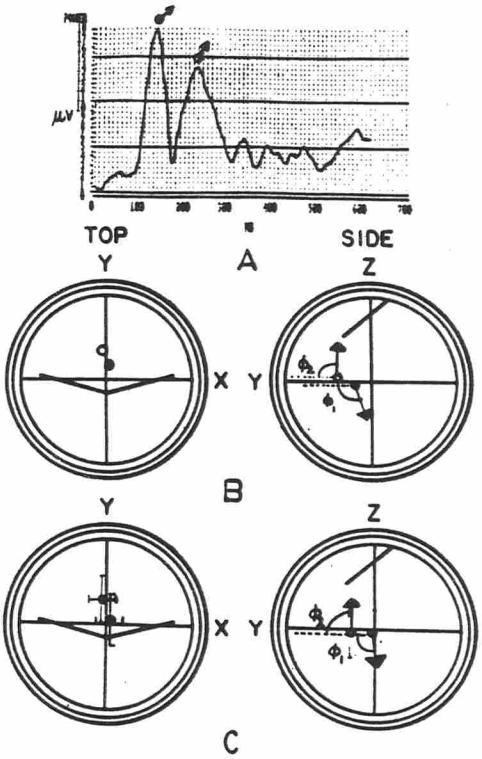

Figure 15

The following table is a synopsis of resting auditory EP results for the 22 normal subjects:

Component	n	Latency	x	y	z
N100	21	113.9 ms	.02	.05	-.03
		(16.6 ms)	(.14)	(.26)	(.23)
		ϕ_1 = 107.6° (13.2°)			
P200	18	197.6 ms	-.08	.23	-.06
		(17.0 ms)	(.13)	(.22)	(.24)
		ϕ_2 = 91.9° (20.7°)			

Table for Normative Resting AER

Numbers in parentheses are standard deviations.

The figures which follow show three-dimensional perspectives, scalp and cortical surface topographies for N100 (Figure 16A) and P200 (Figure 16B).

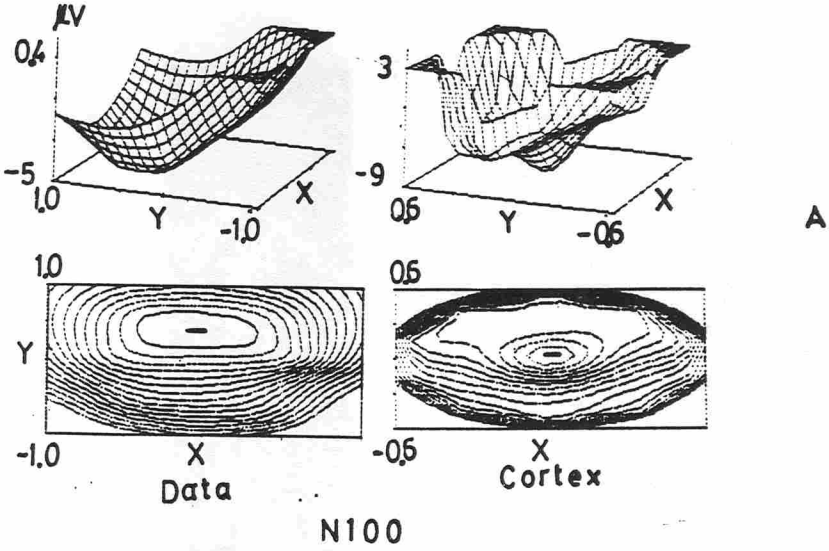

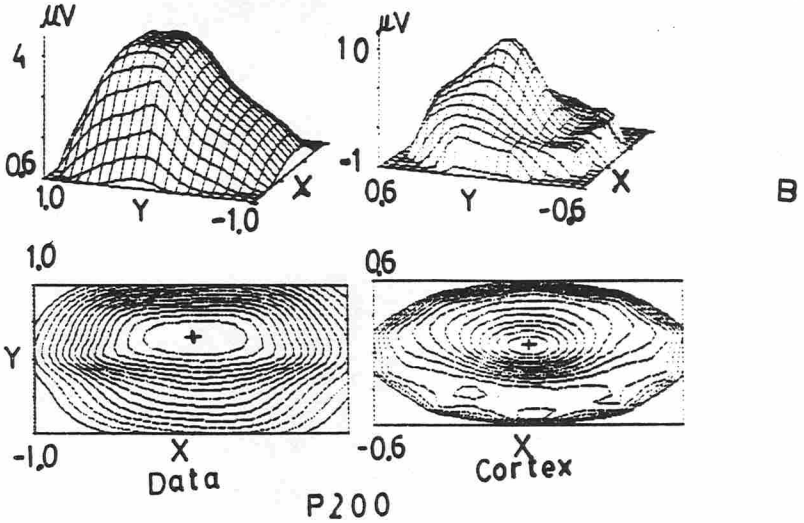

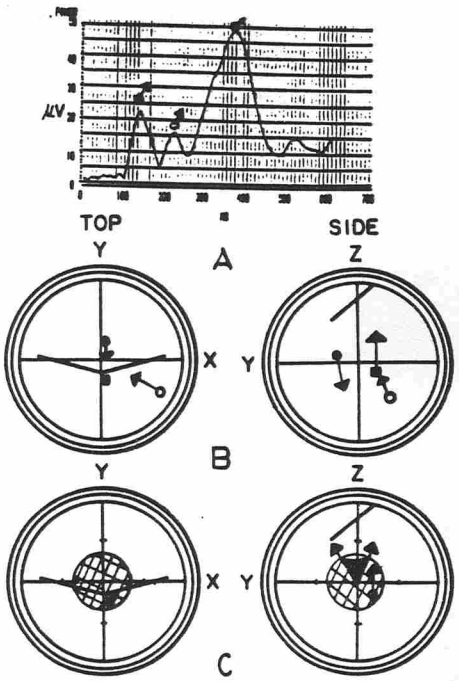

Figure 17

The preceding figures show the power curve for the P300 auditory response for the grand average data for the 22 subjects (Figure 17A), the dipole sources for the grand average data (Figure 17B), and the average P300 equivalent dipole source for the 22 subjects (Figure 17C). The shaded region is where this average dipole lies. All 22 normal subjects exhibit this P300 response. The average latency and power of this component are 330.3 ms (16.9 ms) and 63.7 μv (28.2 μv), respectively. This average dipole is centrically located, 0.30 units (.14) from the center of the sphere, and the angle this average dipole makes with the z-axis is 22.1° (15.6°). The numbers in parentheses are standard deviations.

Figure 18 shows the three-dimensional perspectives, scalp and cortical surface topographies for the "normal" P300 response.

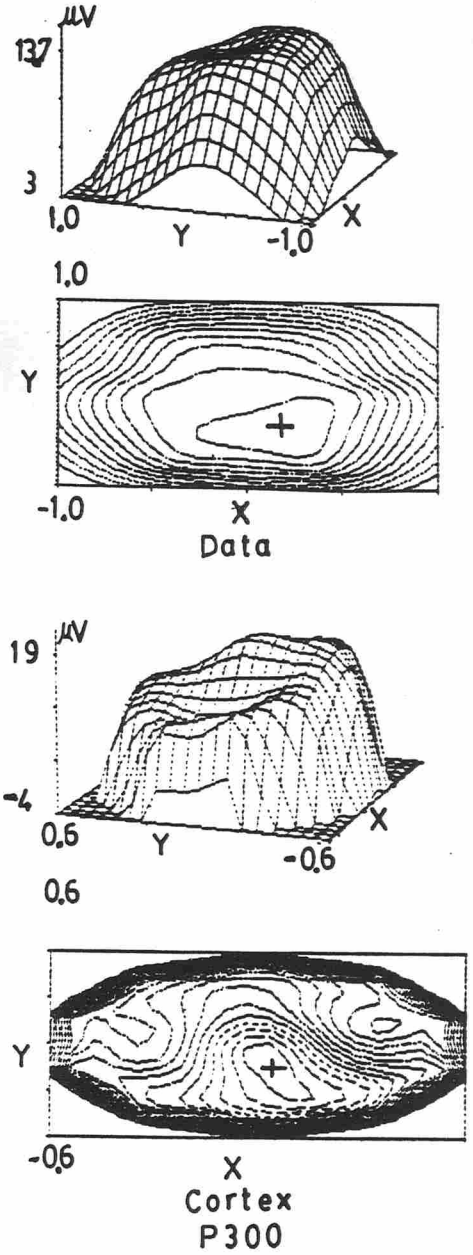

Figure 18

We conclude this section by presenting the P300 results for a normal subject "RITA" and a psychiatric inpatient "WALT" (cf. Figure 12).

The DLM solution for WALT is abnormal because the dipole is superficial ($p < 0.05$) and the angle between the dipole and the z-axis is off ($p < 0.05$). The scalp topography is unremarkable and not qualitatively different from that of RITA. However, the

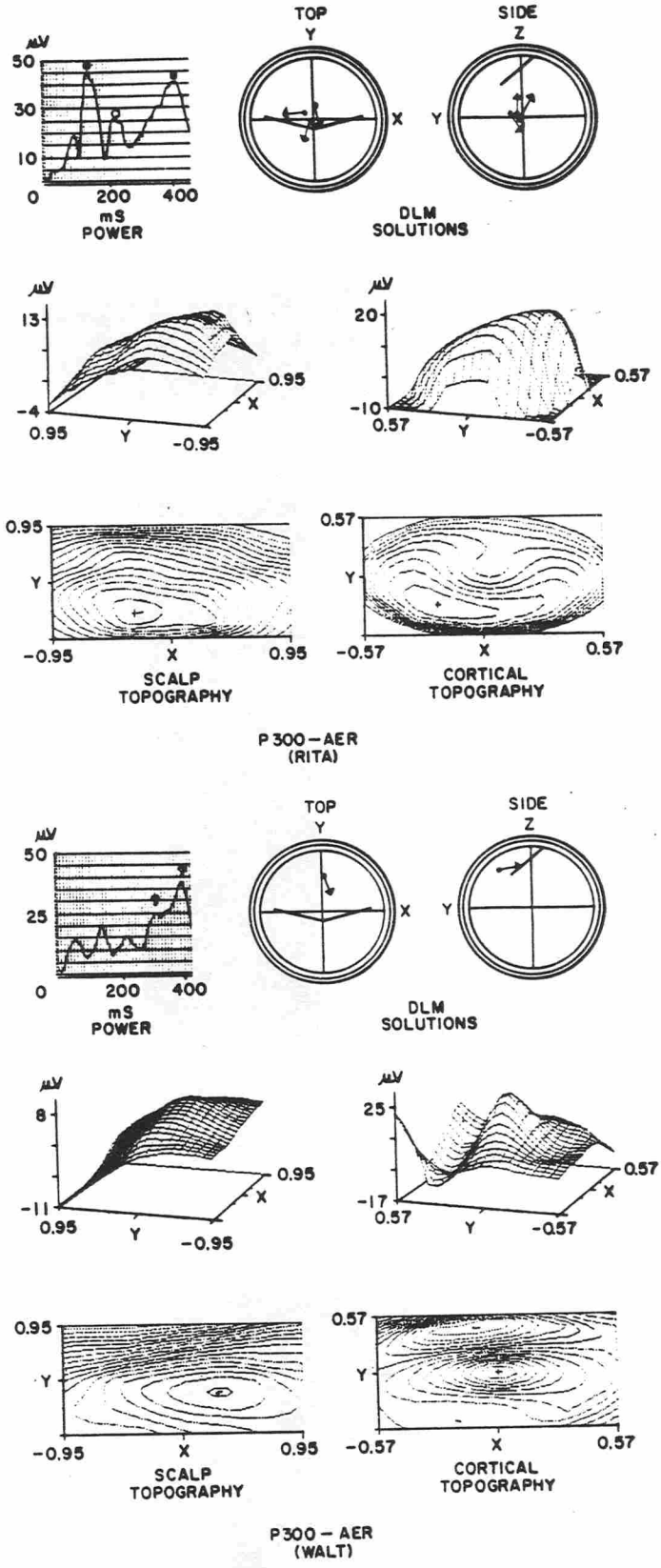
μV
50
30
10
0
200
400
mS
POWER
TOP
Y
X
SIDE
Z
Y
DLM
SOLUTIONS
μV
13
-4
0.95
Y
-0.95
X
0.95
μV
20
-10
0.57
Y
-0.57
X
0.57
0.95
Y
-0.95
X
0.95
SCALP
TOPOGRAPHY
0.57
Y
-0.57
X
0.57
CORTICAL
TOPOGRAPHY
P300-AER
(RITA)
μV
50
25
0
200
400
mS
POWER
TOP
Y
X
SIDE
Z
Y
DLM
SOLUTIONS
μV
8
-11
0.95
Y
-0.95
X
0.95
μV
25
-17
0.57
Y
-0.57
X
0.57
0.95
Y
-0.95
X
0.95
SCALP
TOPOGRAPHY
0.57
Y
-0.57
X
0.57
CORTICAL
TOPOGRAPHY
P300-AER
(WALT)

Figure 19

cortical surface topography is quite different from the normal cases, and suggests multiple superficial neural generators for this component.

6.4. The Response to Pattern-Reversal Visual Stimulation

The following figures depict the power curve for the grand average visual evoked response derived from 21 normal subjects, and the dipole sources for the principal VER components, N1 (88 ms), P1 (122 ms), N2 (156 ms), and P2 (212 ms).

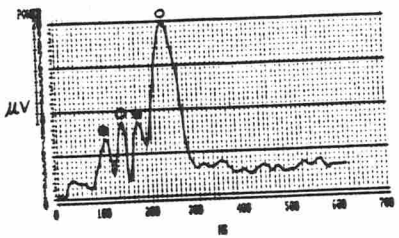

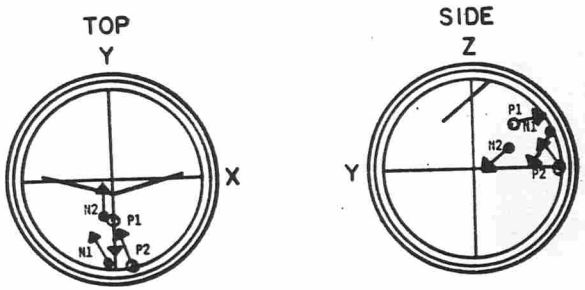

DLM Source for Grand Average Data (N = 22)
Pattern-Reversal Evoked Response

N1 (88 ms), N2 (156 ms)
P1(122 ms), P2 (212 ms)

Figure 20

Figure 21 shows the scalp topographies of these components and Figure 22 shows their cortical topographies. In all of these cases note the increased detail and increased amplitudes in the cortical surface maps.

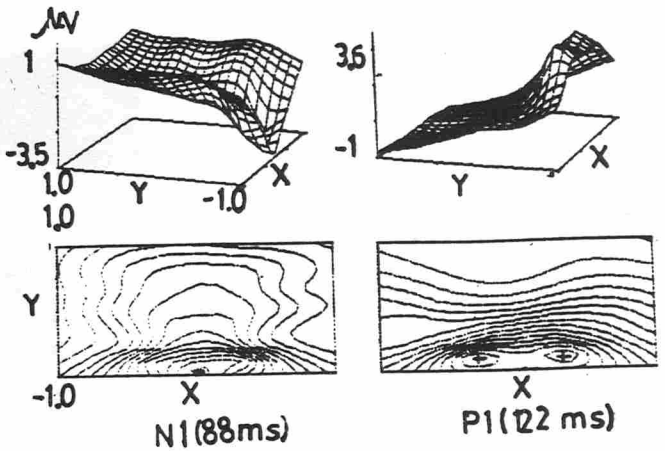

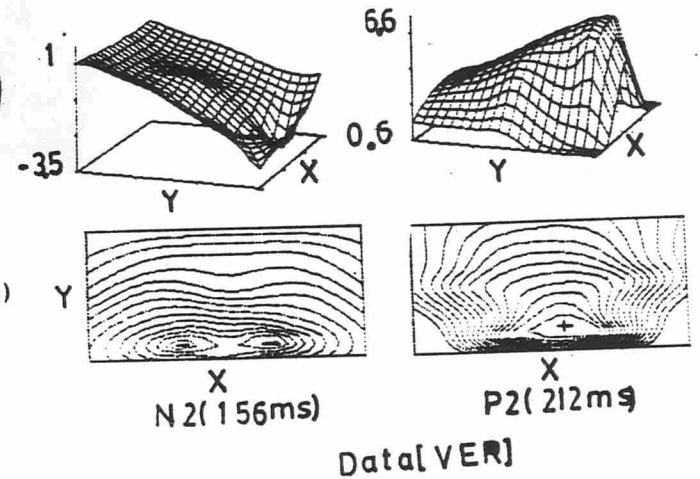

Figure 21

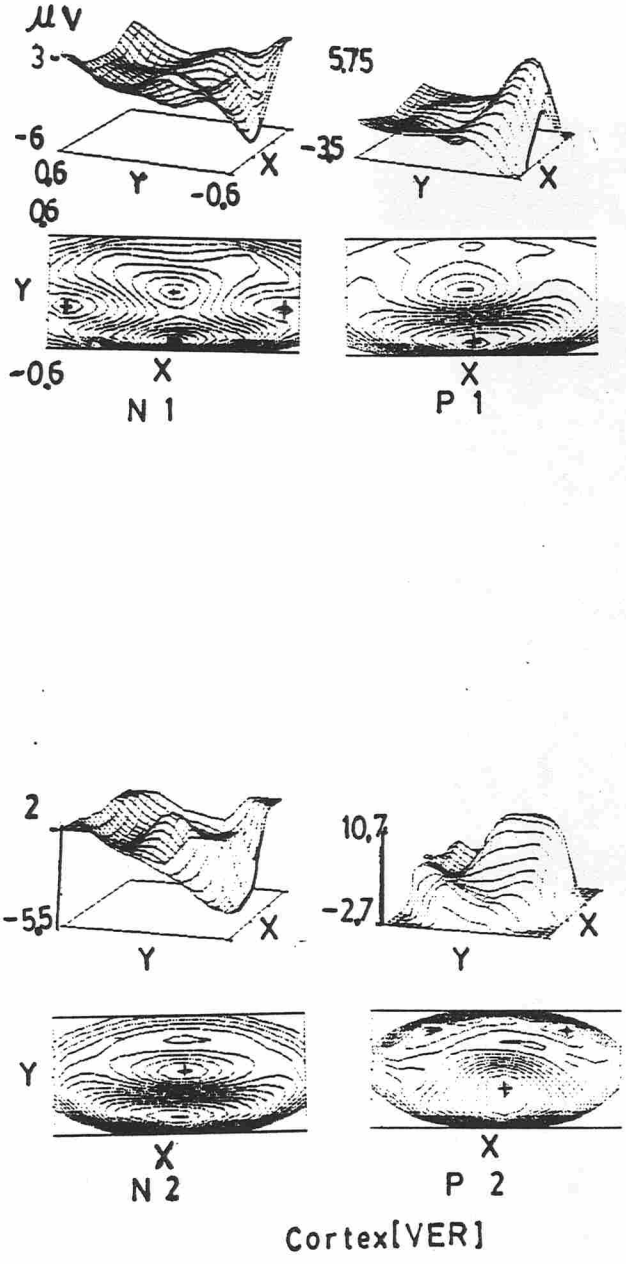

Figure 22

We conclude this section by presenting the VER for an alcoholic subject "TUC." The DLM equivalent source for the first power maximum is too centric ($p < 0.05$) for a supposed cortical generator. The cortical surface topography is clearly different from the normative results presented above. However, the scalp topography is unremarkable, and would be considered statistically normal by the Brain Imager.

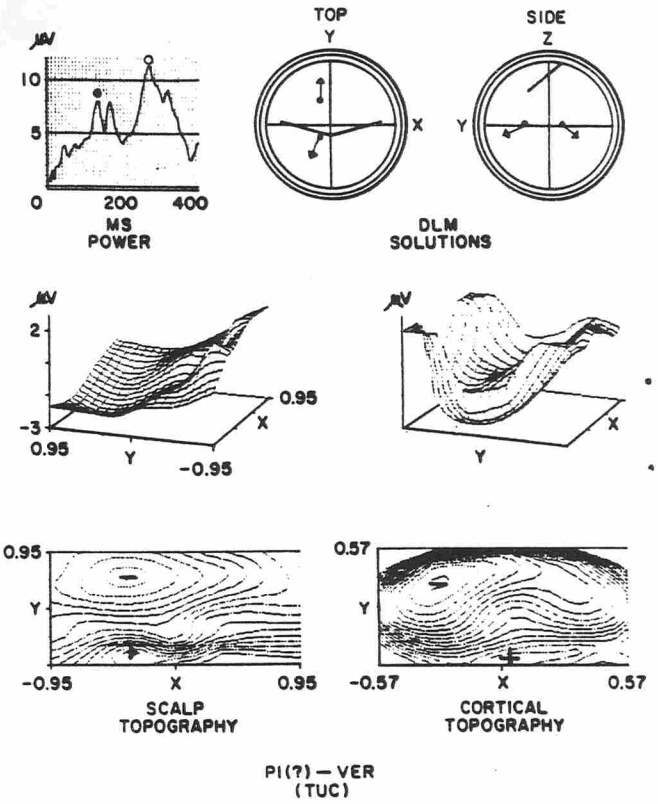

Figure 23

6.5. Conclusions

Although correlations do exist between certain evoked waveforms of their topographical distributions on the one hand, and certain states of consciousness or abnormal brain activity on the other, these correlations are usually limited to inferences derived from the latencies or amplitudes of a few replicable EP components. In this section DLM and CIT have been applied to scalp recorded auditory and visual evoked potentials in order that one might draw conclusions concerning the neural generators of these potentials. DLM appears to be sensitive in distinguishing

between normal and abnormal responses and CIT suggests why a DLM result is abnormal, such as multiple or extended neural generators or generators whose location and/or orientation do not coincide with the location and orientation of the presumed neural sources of the potentials.

7. APPLICATIONS OF DLM TO THE LOCALIZATION OF EPILEPTIC FOCI

As we noted in the Abstract, it is desirable to develop methods which allow the accurate, noninvasive localization of epileptic foci. In the studies described in this section the accuracy of spike localization by the dipole localization method was assessed by comparing the location of the equivalent dipole source with the localization of the focus as identified by intracranial EEG recordings and MRI scans.

7.1. Procedure

The acquisition and analysis of these cases were done at Good Samaritan Hospital, Portland, Oregon. Data recorded from a 16-channel referential montage using the international 10-20 electrode placements were digitized with a 12 bit A/D converter at a frequency of 200 Hz and recorded on both a VHS tape system and a DEC 11/73 computer system. To eliminate artifacts the epoch of EEG to which the DLM technique was applied was selected visually. A two hundred millisecond epoch before and after the peak negativity of the highest amplitude spike was analyzed. In order to assess the effect of "background" noise on spike localization different epochs with similar morphological characteristics were averaged. To align all channels for averaging the channel with the most characteristic spike among the sixteen was chosen as the trigger channel. The DLM technique was then applied to this "averaged" data over the same 400 msec epoch. The result was then compared to single spike localization.

7.2. Subjects

The two subjects in this study suffered from complex partial seizures (CPS). The first subject was a 9 year old female with CPS since age 8 months. Minimal improvement occurred after a conservative left frontal lobectomy in 1985. Pathology showed a forme fruste of tuberous schlerosis (LF in Figure 24).

The second subject was a 45 year old male with CPS since age 12 years. Development was normal until encephalitis occurred at age 5 years. The MRI scan shows a right anterior (RF in Figure 27) temporal lobe lesion.

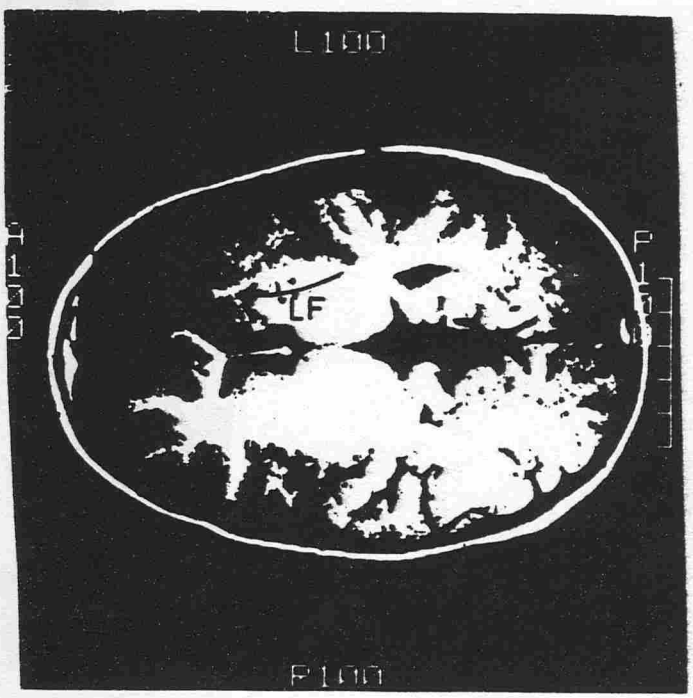

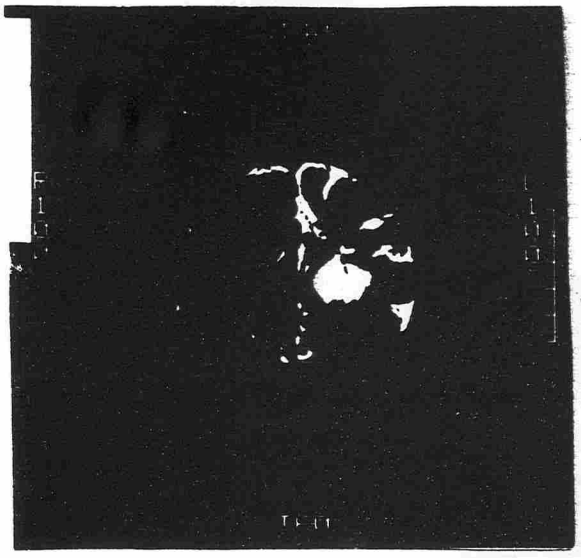

Figure 24

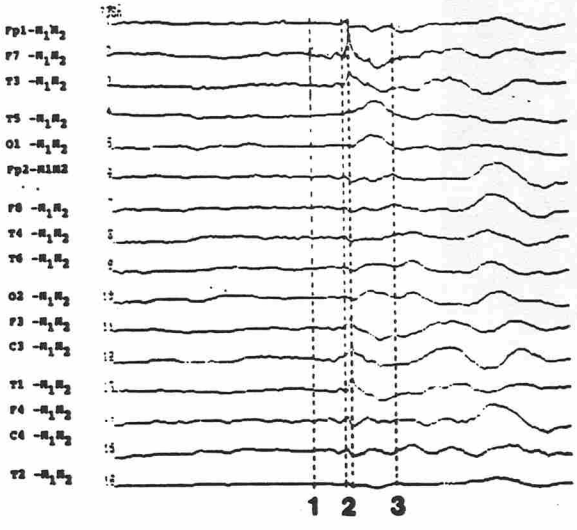

Figure 25

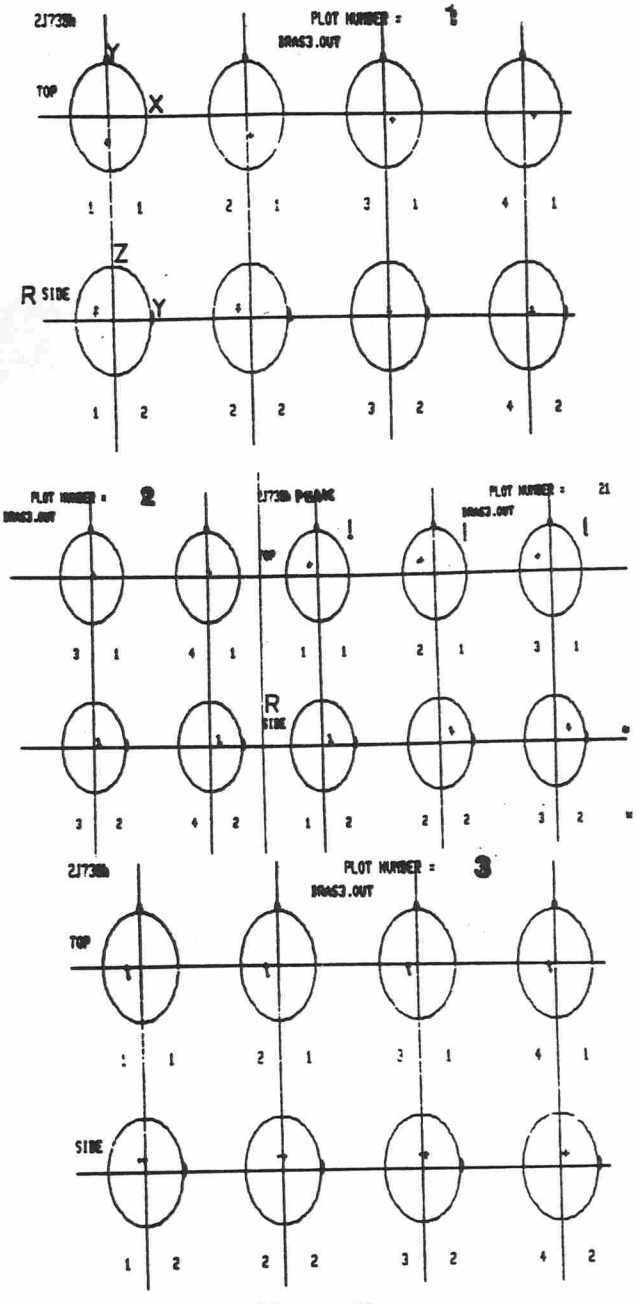

Figure 26

7.3. Results

The four hundred msec epoch containing the spike for the first subject is shown in Figure 25. Figure 26 shows the dipole source for the scalp-recorded data at 10 msec intervals in sequence. The bold numbers correspond to times before, during, and after the epileptiform discharge, as shown in Figure 25. Note that, unlike previous figures in this paper, the 'right' side view is depicted. Also, in the magnetic resonance scans, L = left, R = right, P = posterior, and A = anterior. In the row of figures corresponding to epoch 2, the dipole source does lie in the left frontal quadrant. We have emphasized this result by an exclamation point ! .

The analogous results for the second subject are shown in Figures 28 and 29.

Figure 27

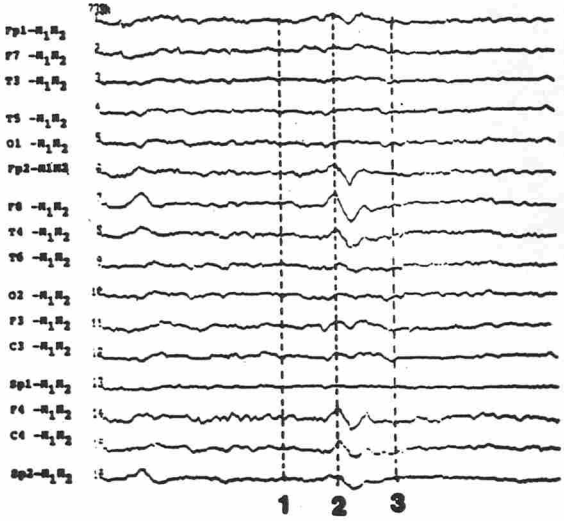

Figure 28

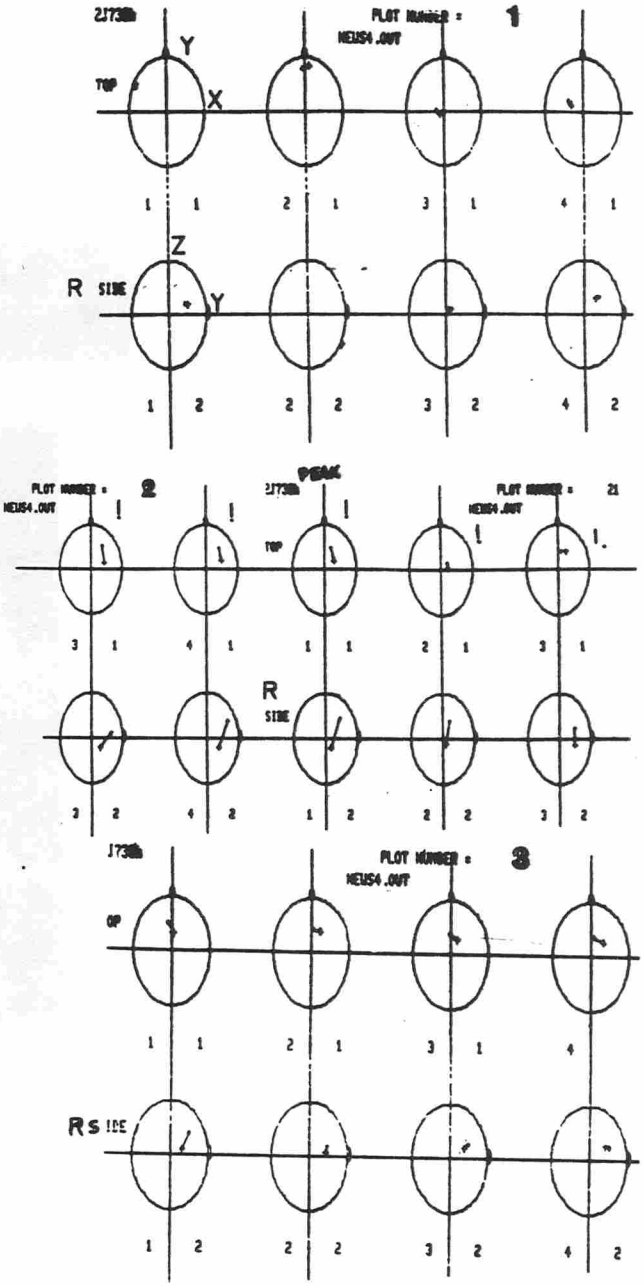

Figure 29

7.4. Discussion

In these cases we found that just prior to and at the peak of the spike the localization was most accurate. The location and orientation of the dipole remained stable for up to 70 msec. The dipole location and its associated moment vectors agreed with intracranial EEG localization and with structural lesions seen on MRI. We found that DLM was not only able to localize superficial foci, but was able to detect spikes arising in the mesial temporal area. In these preliminary studies, "averaging" did not seem to improve the accuracy of localization, but did improve its stability. By eliminating the contributions of random noise, the averaging technique may make it possible to obtain localizing information in cases where the amplitude of the background activity is similar to the amplitude of the spike discharge.

REFERENCES

[1] Sidman, R.D., Giambalvo, V., Allison, T., and Bergey, P., A method for localization of sources of human cerebral potentials evoked by sensory stimuli, Sensory Processes 2 (1978) 116-129.

[2] Sidman, R.D., The time-dependent equivalent dipole source for the response to median nerve stimulation, IEEE Trans. Biomed. Eng., 31 No. 6 (1984) 481-483.

[3] Smith, D.B., Sidman, R.D., Henke, J.S., Labiner, D., and Flanigin, H., A reliable method for localizing deep intracranial sources of the EEG, Neurology 35 No. 12 (1985) 1702-1707.

[4] Lee, L., Smith, D.B., Sidman, R.D., and Kramer, R., Intracranial localization of epileptic spikes using DLM, J. Clin. Neurophysiol., 5 No. 4 (1988) 336 (abstract).

[5] Lehmann, D., Darcey, T.M., and Skrandies, W., Intracerebral and scalp fields evoked by hemiretinal checkerboard reversal and modeling of their dipole generators, in: Courjon, J., Mauguire, F., and Revol, M. (eds), Clinical Applications of Evoked Potentials in Neurology (Raven Press, New York 1982), pp. 41-47.

[6] Ducati, A., Fava, E., and Motti, E., Neuronal generators of the visual evoked potentials: Intracerebral recording in awake humans, Electroenceph. clin. Neurophysiol., 71 (1988) 89-99.

[7] Wood, C.C., McCarthy, G., Squires, N.K., Vaughan, H.G., Woods, D.L., and McCallum, W.C., Anatomical and physiological substrates of event-related potentials: Two case studies, in: Karrer, Cohen, and Tueting (eds), 1984 Annals of the New York Academy of Sciences, Vol. 425, Brain and Information: Event-related Potentials, 681-721.

[8] Sutherling, W.W., Crandall, P.H., Engel, J., Darcey, T.M., Cahan, L.D., and Barth, D.S., The magnetic field of complex partial seizures agrees with intracranial localizations, Annals of Neurology 21 (1987) 545-558.

[9] Wilson, F.N. and Bayley, R.H., The electric field of an eccentric dipole in a homogeneous spherical conducting medium, Circulation 1 (1950) 84-92.

[10] Brody, D.A., Terry, F.H., and Ideker, R.E., Eccentric dipole in a spherical medium: Generalized expression for surface potentials, IEEE Trans. Biomed. Eng. 20 (1973) 141-143.

[11] Ary, J.P., Klein, S.A., and Fender, D.H., Location of sources of evoked scalp potentials: Corrections for skull and scalp thicknesses, IEEE Trans. Biomed. Eng. 28 (1981) 447-452.

[12] Scherg, M., Spatio-temporal modelling of early auditory evoked potentials, Rev. Laryngol (Bordeaux) 105 (1984) 163-170.

[13] Lehmann, D. and Skrandies, W., Reference-free identification of components of checkerboard-evoked multichannel potential fields, Electroenceph. clin. Neurophysiol. 48 (1980) 609-621.

[14] Kavanagh, R.N., Darcey, T.M., and Fender, D.H., The dimensionality of the human visual evoked scalp potential, Electroenceph. clin. Neurophysiol., 40 (1976) 633-644.

[15] Sidman, R.D. and Smith, D.B., Localization of the neural generators of scalp-recorded potentials by means of mathematical models, in: J. Eisenfeld and M. Witten (eds), Modelling of Biomedical Systems (Elsevier Science Publishers 1986) 205-211.

[16] Sidman, R.D., Kearfott, R.B., and Schlichting, C., The inverse problem of electroencephalography assuming double layer neural generators, Proceedings of the IMACS 1988 World Congress, 3, 726-728.

[17] Scherg, M. and Von Cramon, D., Two bilateral sources of the late AEP as identified by a spatio-temporal dipole

model, Electroenceph. clin. Neurophysiol., 62 (1985) 32-44.

[18] Cannon, J.R., Some numerical results for the solution of the heat equation backward in time, in: Greenspan, D. (ed), Numerical Solutions of Nonlinear Differential Equations (John Wiley and Sons 1967), 21-54.

[19] Stewart, G.W., Introduction to Matrix Computations, (Academic Press, New York 1973) 317-326.

[20] Hill, C.D., Kearfott, R.B., and Sidman, R.D., The inverse problem of electroencephalography using an imaging technique for simulating cortical surface data, Proceeding IMACS 1988 3, R. Vichnevetsky, P. Borne, J. Vignes (eds) 729-731.

[21] Sutton, S., Braren, M., Zubin, J., and John, E.R., Evoked potential correlates of stimulus uncertainty, Science 150 (1965) 1187-1188.

[22] Morstyn, R., Duffy, F., and McCarley, R., Altered P300 topography in schizophrenia, Archives of General Psychiatry, 40 (1983) 729-734.

[23] Faux, S. Torello, M., McCarley, R., Shenton, M., and Duffy, F., P300 in schizophrenia: Confirmation and statistical validation of temporal region deficit in P300 topography, Biological Psychiatry (in press).

[24] McCarthy, G., Darcey, T.M., Wood, C.C., Williamson, P.D., and Spender, D.D., Asymmetries in scalp and intracranial endogenous ERPs in patients with complex partial epilepsy, in: Fundamental Mechanisms of Human Brain Function, J. Engel, Jr. et al (eds) (Raven Press, New York) 1987, 51-59.

[25] Sidman, R.D. and Smith, D.B., Application des potentiels evoques visuels a la localization d'une atteinte neurologique, Innovation et Technologie en Biologie et Medecine 7 No. 3 (1986) 323-330.